Journal of Membrane Science 640 (2021) 119786

Contents lists available at ScienceDirect

Journal of Membrane Science

journal homepage: www.elsevier.com/locate/memsci

Quantifying diffusion of organic liquids in a MOF component of MOF/Polymer mixed-matrix membranes by high field NMR

Amineh Baniani [a], Matthew P. Rivera [b], Ryan P. Lively [b], Sergey Vasenkov [a,*]

[a] Department of Chemical Engineering, University of Florida, Gainesville, FL, 32611, USA
[b] School of Chemical & Biomolecular Engineering, Georgia Institute of Technology, Atlanta, GA, 30332, USA

ARTICLE INFO

Keywords:
Diffusion
PFG NMR
Liquid separations
Mixed-matrix membranes
ZIF-71

ABSTRACT

Confinement of crystals of metal–organic frameworks (MOFs) in polymers to form MOF/polymer mixed-matrix membranes (MMMs) can lead to changes in intra-MOF diffusion. Such changes in intra-MOF diffusion were previously demonstrated for light gases, and attributed to a reduction in MOF framework flexibility. However, to our knowledge, no direct measurements of intra-MOF diffusion in MMMs and of the related MOF confinement effect on diffusion have been reported for organic liquids. In this work, ^{13}C pulsed field gradient (PFG) NMR was used to quantify self-diffusion of methanol, ethanol, *p*-xylene, and *o*-xylene inside MOF crystals of the type ZIF-71, which were dispersed in a Torlon polymer to form MMMs. The intra-ZIF self-diffusivities in the MMMs were compared with the corresponding self-diffusivities measured in beds of ZIF-71 crystals. The observed self-diffusivity dependencies on diffusion time were explained by crystal boundary effects. The corresponding values of intra-ZIF self-diffusivities not perturbed by such effects were found to be the same, within uncertainty, in the MMMs and ZIF-71 beds. The observed lack of an influence of the ZIF-71 confinement in Torlon on diffusion is explained, and an option to increase diffusion selectivity is discussed.

1. Introduction

Mixed-matrix membranes (MMMs), which are composed of porous fillers dispersed in a polymer, have emerged as promising materials for energy-efficient gas and liquid separations. MMMs have shown superior separation performance compared to pure polymeric membranes [1–12]. A large number of studies were performed with the focus on performance of MMMs prepared with different types of inorganic fillers including zeolites [3–5], and carbon molecular sieves (CMS) [6,13,14]. More recently, zeolitic imidazolate frameworks (ZIFs) have also been used as extremely promising molecular sieve fillers in MMM fabrication [7–11,15–18]. ZIFs represent a subclass of metal organic frameworks (MOFs) featuring large surface area, permanent porosity, significant chemical and thermal stabilities, and adjustable pore apertures in the range of about 2–20 Å [19–21]. ZIF/polymer MMMs benefit from tunable molecular sieving properties of ZIFs coupled with the ease of fabrication and low cost of pure polymeric membranes. In recent years, such MMMs were considered also for liquid separations [22–24], in addition to more common applications in gas separations.

Majority of the experimental and simulation studies with ZIF-containing MMMs were carried out with ZIFs of the types ZIF-8, ZIF-11 and ZIF-90, which were utilized for liquid and/or gas separations (see, for example, refs [7–9,22–28]). For reasons discussed below, ZIF-71 is another promising candidate for a filler in MMM fabrications, especially for sorbate molecules appreciably larger than light gases. Until now, only a limited number of transport studies of ZIF-71 based MMMs were reported [29–32]. Porous structure of ZIF-71 is formed by a coordination of tetrahedral zinc metal ions with dichloromidazole ligands yielding a RHO topology [20,33]. ZIF-71 has larger nominal pore aperture size (4.2 Å [19]) than those of ZIF-11 (3.0 Å [20]), ZIF-8 (3.4 Å [19]) and ZIF-90 (3.5 Å [19]). This makes ZIF-71 more attractive for molecular sieving of liquid sorbates exhibiting molecular sizes larger than those of light gases, such as methane and carbon dioxide.

It is well known that due to an existence of framework flexibility of MOF and ZIF materials, sorbates with molecular sizes larger than the nominal pore aperture sizes can gain an ability to diffuse freely in these materials (see, for example, refs [34–41]). Moreover, such framework flexibility can be tailored (reduced) by confining MOF and ZIF crystals in certain polymers to form MMMs [7,15–18,42,43]. In particular, polymers with large bulk moduli have demonstrated this confinement effect, which reduces the molecular diffusion rates inside MOF and/or ZIF crystals. These findings emphasize the importance of quantifying

* Corresponding author.
E-mail address: svasenkov@che.ufl.edu (S. Vasenkov).

https://doi.org/10.1016/j.memsci.2021.119786
Received 17 June 2021; Received in revised form 13 August 2021; Accepted 24 August 2021
Available online 3 September 2021

microscale transport inside MMMs in a manner allowing resolving transport properties of MOF and/or ZIF crystals confined in polymer matrices. We have previously demonstrated the capability of pulsed field gradient (PFG) NMR technique in resolving gas diffusion inside the polymer phases and/or inside ZIF crystals located in ZIF/polymer MMMs [15–18,42]. In particular, in our recent work we utilized PFG NMR to study intra-ZIF self-diffusion of ethane and ethylene in ZIF-11/polymer MMMs formed with three different polymer types as well as in the corresponding loosely packed beds of ZIF-11 crystals. It was observed that confinement of ZIF-11 crystals in Torlon polymer can lead to a reduction in the intra-ZIF self-diffusivity of the studied gases by a factor of about 2, while no such diffusivity reduction was observed for the MMMs formed with the other two studied polymer types. The observed reduction in the intra-ZIF self-diffusion was explained by reduced framework flexibility of confined ZIF-11 crystals in Torlon polymer, which exhibits larger bulk modulus than those of the other two studied polymers [17,18,42]. Although detailed intra-MOF diffusion studies in MMMs have been demonstrated for light gases, such studies were not yet reported for any liquids.

In this work, we demonstrate an ability of high field NMR diffusometry to resolve intra-ZIF self-diffusion inside ZIF/polymer MMMs for liquid sorbates with molecular sizes significantly larger than those of gas molecules previously used in such studies. High field ^{13}C PFG NMR was applied to quantify diffusion of methanol, ethanol, *para*-xylene (*p*-xylene), and *ortho*-xylene (*o*-xylene) inside ZIF-71/Torlon MMMs, i.e. MMMs formed by dispersing crystals of ZIF-71 in Torlon polymer. These sorbates were selected due to their relevance for industrial applications and challenges related to high efficiency membrane-based separations of ethanol/methanol and *p*-xylene/*o*-xylene mixtures. Most of the diffusion studies were performed with the MMMs containing ZIF-71 crystals with an average crystal sizes of 3 μm (batch A). In addition, the corresponding MMMs containing ZIF-71 crystals with an average crystal sizes of 1 μm (batch B) were also investigated. An influence of the external crystals surface of ZIF-71 crystals confined in MMMs on the intra-ZIF self-diffusion was investigated by performing ^{13}C PFG NMR diffusion studies for different diffusion times and the corresponding root mean square displacements (root MSDs) comparable with and smaller than the average crystal sizes. Large magnetic field gradients up to 23 T/m were required for such studies because they afford diffusion measurements to be performed for relatively small length scales of displacements in the sub-micrometer and micrometer ranges. An application of high magnetic field of 14 or 17.6 T was needed to enable sufficiently large signal-to-noise ratios in the measurements of the ^{13}C PFG NMR signal, which suffers from a much lower sensitivity of ^{13}C detection in comparison to that of protons. ^{1}H PFG NMR measurements could not be used due to low ^{1}H T_2 NMR relaxation times of the liquid sorbates in the studied ZIF material. The intra-ZIF self-diffusion data obtained for the MMMs were compared with those measured for beds of batch A crystals. Furthermore, we also report methanol/ethanol and *p*-xylene/*o*-xylene intra-ZIF self-diffusion selectivities for the MMMs and crystal beds, i.e. the ratios of the intra-ZIF self-diffusivities, which are not perturbed by any diffusion restriction effects at the external crystal surface. Due to a complex nature of diffusion in MOF/polymer MMMs, the reported results are expected to be beneficial for future design and optimization of such MMMs for liquid separations.

2. Experimental

2.1. ZIF-71 synthesis

2.1.1. Small crystal (batch B) synthesis

Small ZIF-71 crystals (average crystal size of 1 μm) were synthesized following a procedure reported previously [44]. Briefly, separate solutions of 0.5852 g zinc acetate dihydrate (2.64 mmol) and 1.4608 g 4, 5-dichloroimidazole (10.68 mmol) in 100 mL methanol were prepared. The solutions were sonicated in a sonic bath until complete dissolution. The solutions were combined in a round bottom flask and allowed to sit undisturbed for 24 h. Precipitated solids (viz. ZIF-71 crystals) were isolated by centrifuge. The crystals were soaked in chloroform for three days, replacing with fresh chloroform each day. The crystals were isolated by centrifuge and dried under vacuum at 353 K overnight. The crystal size distribution and a representative SEM image for batch B are shown in Figs. S1 and S2, respectively.

2.1.2. Large crystal (batch A) synthesis

Large ZIF-71 crystals (average crystal size of 3 μm) were synthesized by adding a modulator to the small crystal synthesis. A solution of 0.5852 g zinc acetate dihydrate in 100 mL methanol was prepared. Separate solutions of 1.4608 g 4,5-dichloroimidazole and 0.5816 g imidazole (8.54 mmol) in 50 mL methanol were prepared. All solutions were sonicated until complete solvation. The 4,5-dichloroimidazole and imidazole solutions were combined and then mixed with the zinc solution. The mixture was allowed to sit undisturbed for 48 h. Crystals were isolated by centrifuge and washed with dimethylformamide (DMF) for three days, replacing with fresh DMF each day. Crystals were then washed with methanol for three days, replacing with fresh methanol each day. Crystals were dried at 353 K overnight. The crystal size distribution and a representative SEM image for batch A are shown in Figs. S1 and S2, respectively.

2.2. ZIF-71/Torlon mixed-matrix membrane fabrication

ZIF-71/Torlon MMMs were prepared by the blade casting method. ZIF-71 crystals and Torlon were dried under vacuum at 373 K overnight. 0.7 g ZIF-71 and 0.3 g Torlon were dispersed in 2.5 g N-methyl-2-pyrrolidone (NMP). The dope was mixed on a rolling mixer under a heat lamp at a temperature of approximately 333 K overnight. A clean glass plate was heated to 323 K. The dope was cast on the heated plate and allowed to dry overnight. The film was solvent exchanged with methanol for three days, replacing with fresh methanol each day. The film was then dried at 373 K under vacuum overnight. Fig. S3 shows representative SEM images of the MMMs.

2.3. Powder X-ray diffraction measurements

Powder X-ray diffraction measurements were performed with PANalytical X'Pert PRO Alpha-1 at 40 kV and 40 mA with Cu-Kα radiation of 1.54184 Å over a 2θ range of 2°–30°. Samples were mounted onto a silicon zero background holder. The step size was 0.008356 and the scan time was 40.005 s/step. Spectra are presented in Fig. S4, along with a predicted spectrum from the Cambridge Crystallographic Data Centre, Database Identifier GITVIP, and generated with the crystallographic software Mercury. Peak placement in batch B matches closely with the predicted spectrum. The spectrum of batch A presents a slight shift to the right from the predicted spectrum. This shift, however, is very minor, and the spectrum appears to be in otherwise good agreement with the predicted one. Hence, we conclude that both batches A and B correspond to ZIF-71.

2.4. NMR samples preparation

NMR samples with MMMs were prepared by placing tightly packed strips of ZIF-71/Torlon MMM into 5 mm thin wall NMR tubes (Wilmad Labglass, Inc.) to reach a height in the tubes of about 30 ± 5 mm. In these samples, the membrane external surface was perpendicular to the radial direction of the tubes. Similarly, NMR samples with ZIF-71 crystal beds were prepared by placing ZIF-71 crystals into the same type of NMR tubes to obtain loosely packed beds of ZIF-71 crystals with a height of about 20 ± 5 mm. Using a custom-made vacuum system, samples were activated at 373 K for 10 h under high vacuum to become sorbate free. Following activation, the samples were left under high vacuum without heating until they cool down to an ambient temperature of around 298

K. Once the ambient temperature was reached, the samples were loaded with a one component liquid sorbate. The sorbates selected for this work were ^{13}C-labeled methanol (Sigma-Aldrich), $^{13}C_2$-labeled ethanol (Sigma-Aldrich), $^{13}C_2$-labeled *p*-xylene (Sigma-Aldrich) and $^{13}C_2$-labeled *o*-xylene (Sigma-Aldrich). All the liquid sorbates consisted of a 99% isotopic purity. In all cases, a sufficient amount of sorbate was cryogenically transferred from the vapor phase of the calibrated volume of the vacuum system to achieve sorption equilibrium of the MMMs or ZIF-71 beds with the sorbate at the saturation vapor pressure at ambient temperature (~298 K). After sorbate loading, the sample tubes containing porous materials and liquid sorbates were flame sealed. The desired sorption equilibrium conditions were ensured by transferring enough liquid into each sample tube so that a small amount of liquid sorbate was still present in the tube even after several days of equilibration at 298 K, as well as after equilibration at other temperatures used in our NMR measurements. It is important to note that as a result of the loading and equilibration procedure discussed above, the intra-ZIF sorbate concentrations in the MMM and the corresponding ZIF-71 bed samples should be the same for each particular sorbate and temperature used because this concentration corresponds to the sorption equilibrium conditions at saturation vapor pressure in the surrounding gas phase.

An area under a ^{13}C NMR spectrum of sorbate molecules (i.e. NMR signal intensity), which is proportional to the number of sorbate molecules in a sample, was used to estimate the sorbate amount in this sample. The proportionality factor between the amount of sorbate and the corresponding NMR signal intensity was obtained from measurements of a reference sample containing only a known amount of the respective bulk liquid sorbate where no porous material was present. This approach was also used in our previous work [17,18,45]. To estimate the intra-ZIF concentration for each studied sorbate under our experimental conditions, we used an expected difference between the ^{13}C T_2 NMR relaxation time of sorbate molecules located inside ZIF-71 crystals and that for the liquid sorbate outside the crystals in the ZIF-71 bed samples. Our ^{13}C T_2 NMR relaxation measurements allowed obtaining these T_2 NMR relaxation times and the related sorbate fractions, as discussed below and in supplementary materials section. Multiplying the fraction of the intra-ZIF component with the total sorbate amount in a bed sample we estimated the intra-ZIF sorbate concentration in the sample. These concentration estimates at 296 K are given in Table 1 for all studied sorbates. Based on our NMR data and sample preparation procedure, the corresponding intra-ZIF concentration in the studied MMMs should be the same as those in the beds, within uncertainty.

2.5. NMR measurements

^{13}C NMR measurements were carried out using a 51 mm/14 T Avance III spectrometer (Bruker Biospin) and an 89 mm/17.6 T Avance III HD spectrometer (Bruker Biospin) operating at ^{13}C resonance frequencies of 149.8 MHz and 188.6 MHz, respectively. Most of the diffusion data were obtained at 14 T, and only selected measurements were performed under the same or similar experimental conditions at 17.6 T to verify the data measured at 14 T. The observed coincidence of the data measured with the same samples at 14 T and 17.6 T confirmed the absence of any measurement artifacts, including possible effects of magnetic susceptibility, as discussed below. ^{13}C PFG NMR was used for diffusion measurements to take advantage of larger T_2 NMR relaxation times of ^{13}C nuclei than ^{1}H nuclei of guest molecules confined in microporous solids. For methanol, *p*-xylene, and *o*-xylene, the ^{13}C NMR spectrum consists of a single line with the chemical shifts of around 50, 21, and 20 ppm, respectively. For ethanol, the ^{13}C NMR spectrum exhibits two lines with chemical shifts of around 58 and 19 ppm. An NMR reference standard of 40% 1,4-dioxane in benzene-d_6 (Sigma-Aldrich) was used as a reference for the ^{13}C NMR chemical shift determination.

Table 1
Intra-ZIF sorbate loadings of methanol, ethanol, *p*-xylene and *o*-xylene in ZIF-71 crystal bed samples obtained by NMR signal analysis at 296 K.

Sorbate	Sorbate loading (mmol/g)[a]
Methanol	10.8
Ethanol	6.7
P-xylene	1.2
O-xylene	1.1

[a] 20–30% experimental uncertainty.

Sine-shaped magnetic field gradient pulses with strengths up to 18 T/m and 23 T/m were generated, respectively, using *diff30* diffusion probe (Bruker Biospin) at 14 T and *diff50* diffusion probe (Bruker Biospin) at 17.6 T. Magnetic field gradient durations were between 0.5 ms and 2 ms. A total time needed to measure a single intra-ZIF self-diffusivity by ^{13}C PFG NMR varied between 1 and 7 h with the total number of scans ranging from 64 to 256. The repetition delays were chosen to be between 3 and 16 s. They were at least 1.5 times greater than the corresponding T_1 relaxation times. Before any measurements, samples were kept inside the magnet for at least 1 h at a chosen measurement temperature to ensure sorption equilibrium. During the measurements, selected PFG NMR experiments were repeated after waiting times of at least several hours at the same temperature to ensure that the measurement results remain the same, thus indicating no changes in the samples, including no changes in the intra-ZIF sorbate concentration.

Diffusion experiments were carried out using the 13-interval and, in a few cases, stimulated echo PFG NMR pulse sequences with sine-shaped magnetic field gradients and a longitudinal eddy current delay [46,47]. The magnetic field gradient induced attenuation of the PFG NMR signal (Ψ), which is determined by the normalized PFG NMR signal intensity (S) measured as a function of the gradient amplitude (g), was used to obtain self-diffusion coefficients (D). PFG NMR signal attenuation for one molecular ensemble diffusing with a single self-diffusivity D can be presented as [46,48–52].

$$\Psi = \frac{S(g)}{S(g \approx 0)} = \exp\left(- \frac{< r^2(t) > q^2}{6} \right) = \exp\left(- Dtq^2 \right) \quad (1)$$

where $< r^2 >$ is the MSD, $q = \gamma g \delta$, γ is the gyromagnetic ratio, δ is the normalized magnetic field gradient durations, and t is the diffusion time defined in refs. [46,52,53]. For three-dimensional diffusion, MSD can be written using Einstein relation as [48].

$$< r^2 (t) >= 6Dt. \quad (2)$$

In the case of two molecular ensembles diffusing with different self-diffusivities, the relation for the PFG NMR signal attenuation, Eq. (1), can be re-written as [48–50].

$$\Psi = \frac{S(g)}{S(g \approx 0)} = \sum_{i=1}^{2} p_i \exp\left(- D_i q^2 t \right) \quad (3)$$

where p_i is a population fraction (i.e. fraction of the PFG NMR signal) and D_i is the corresponding self-diffusivity of ensemble *i*. The experimental error in self-diffusivities was determined by consideration of the following factors: reproducibility of the diffusion data measured at magnetic fields of 14 T and 17.6 T under identical measurement conditions with the same NMR samples, and reproducibility of the diffusion data measured with different NMR samples prepared in the identical way.

Longitudinal (T_1) and transverse (T_2) NMR relaxation times of the sorbates in the studied samples were estimated using standard inversion recovery and standard Carr-Purcell-Meiboom-Gill (CPMG) pulse sequences, respectively. In CPMG pulse sequence, tau was chosen to be 100 μs. Inversion recovery measurements yielded relaxation data, which indicate an existence of a single T_1 NMR relaxation time for all sorbate molecules in each studied sample. Tables S1 and S2 show results of the

T_1 NMR relaxation time measurements. CPMG data were found to be consistent with the existence of two ensembles of sorbate molecules with different T_2 NMR relaxation times in each studied sample. A bi-exponential fit of the CPMG data allowed obtaining molecular fractions for each ensemble, in addition to the relaxation times. Two ensembles observed for each sample were attributed to sorbate molecules outside of ZIF-71 crystals and/or MMM samples (ensemble 1) and those inside ZIF-71 crystals (ensemble 2). For the MMM samples, no additional T_2 ensemble corresponding to sorbate molecules in the polymer phase of MMMs was observed. The lack of observation of such an ensemble is consistent with the previous measurements of gas molecules in Torlon-based MMMs [17,18,42], and can be explained by very small fraction and T_2 NMR relaxation time of such ensemble in comparison with those of the other two ensembles (see supplementary materials section for more details). Results of the T_2 NMR relaxation time measurements are shown in Tables S1 and S2.

3. Results and discussion

3.1. Measured PFG NMR attenuation curves

Figs. 1 and 2 present examples of ^{13}C PFG NMR attenuation curves for sorbate diffusion in ZIF-71 crystal beds and ZIF-71/Torlon MMMs, respectively. These data were measured at 14 T for methanol and ethanol diffusion at 253 K and for *p*-xylene and *o*-xylene diffusion at 273 K. Additional examples of measured ^{13}C PFG NMR attenuation curves for methanol, ethanol, *p*-xylene and *o*-xylene diffusion in ZIF-71 crystal beds and ZIF-71/Torlon MMMs at different temperatures are presented in supplementary materials (Figs. S5–S9). In addition to the MMMs formed with 3 μm ZIF-71 crystals (batch A), the corresponding MMMs

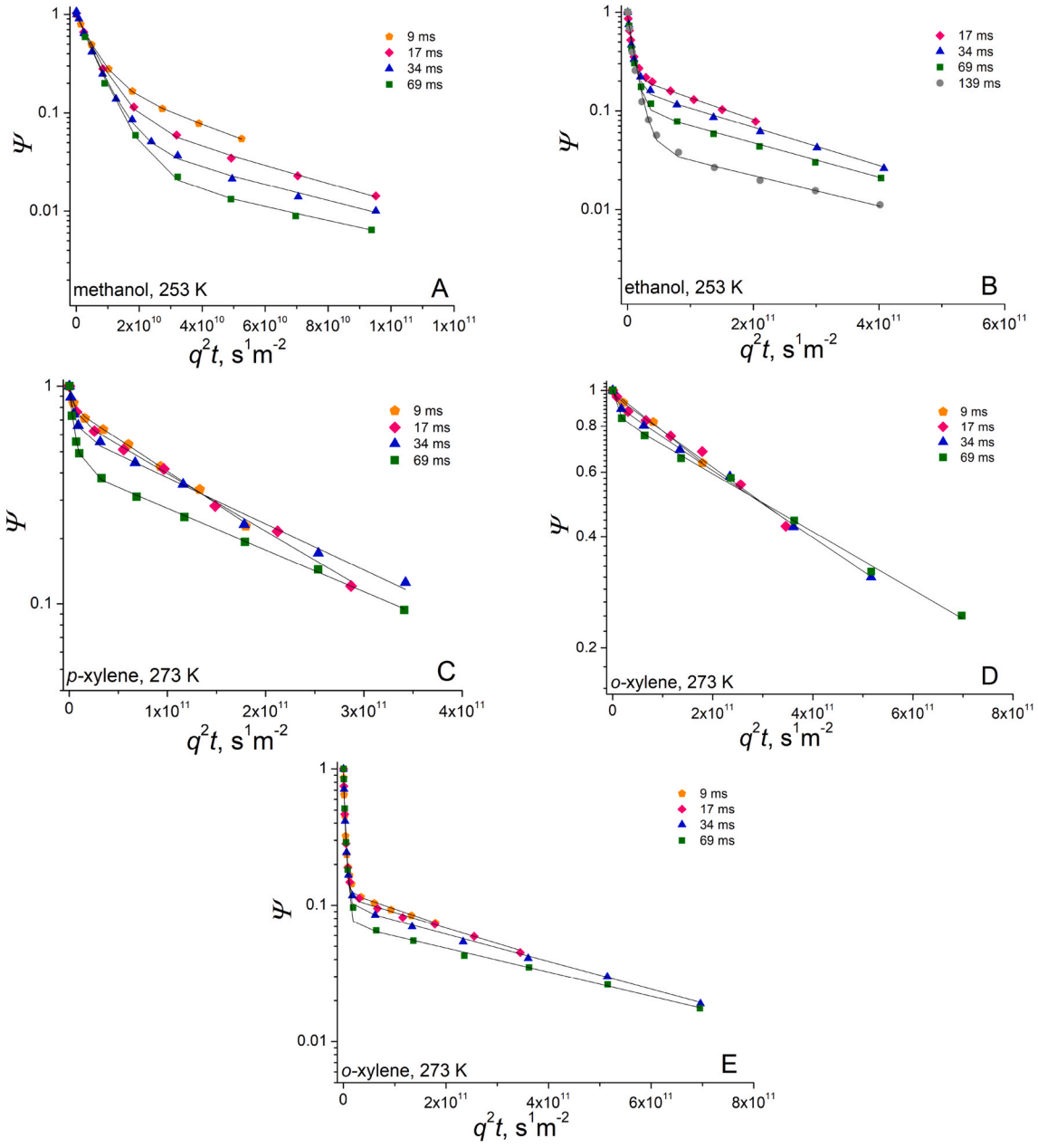

Fig. 1. ^{13}C PFG NMR attenuation curves measured with the samples of beds of ZIF-71 crystals (batch A) loaded with methanol (A), ethanol (B), *p*-xylene (C), and *o*-xylene (D,E). The measurements were performed using the 13-interval PFG NMR pulse sequence at 14 T for different diffusion times and at different temperatures shown in the figure. The solid lines show the results of least-square fitting using Eq. (3). Data shown in E correspond to more o-xylene in the sample tube than that shown in D. Here and later the size of points in the PFG NMR attenuation plots indicates the experimental uncertainty.

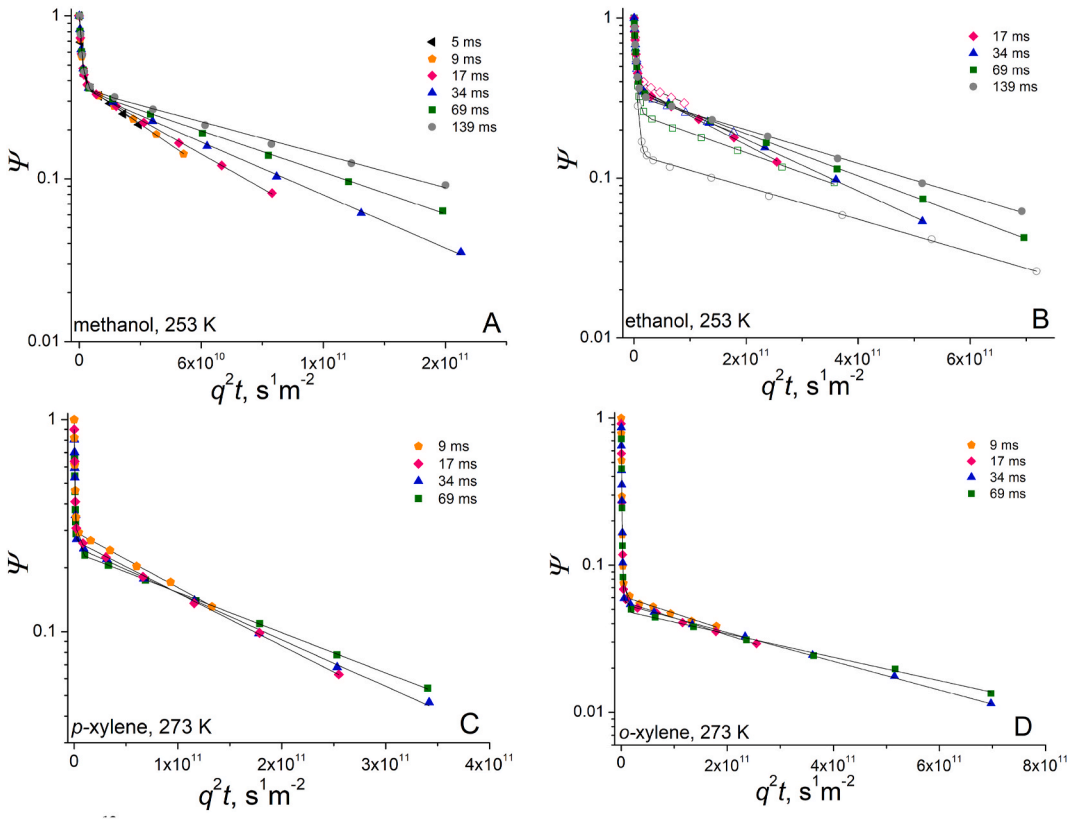

Fig. 2. ^{13}C PFG NMR attenuation curves measured in ZIF-71/Torlon MMM samples for the self-diffusion of methanol (A), ethanol (B), *p*-xylene (C), and *o*-xylene (D) for different diffusion times and at different temperatures shown in the figure. The measurements were performed using the 13-interval PFG NMR pulse sequence at 14 T (filled symbols). Also shown for comparison are the results of additional ^{13}C PFG NMR measurements for ethanol (B) that were performed using the stimulated echo PFG NMR pulse sequence at 14 T (empty symbols). The solid lines show the results of least-square fitting using Eq. (3). The data correspond to ZIF-71/Torlon MMMs containing ZIF-71 crystals with the average crystal size of 3 μm (batch A).

prepared with 1 μm ZIF-71 crystals (batch B) were also used in our diffusion studies (Fig. S10). Although ^{13}C PFG NMR measurements of the MMM samples with batch B were possible, such measurements with crystal beds of batch B were prevented by low signal-to-noise ratios of the ^{13}C PFG NMR signal. The low signal-to-noise ratios are the consequence of small T_2 NMR relaxation times of sorbate molecules in the batch B bed samples (Table S1). These small T_2 NMR relaxation times are attributed to an enhanced influence of the magnetic susceptibility effects, which are expected to be larger for smaller crystals. In contrast to the crystal beds, in MMMs ZIF-71 crystals are surrounded by a polymer phase with the magnetic susceptibility not very different from that of the ZIF material.

Although most of the diffusion measurements were performed at 14 T, some complementary ^{13}C PFG NMR measurements were carried out at a larger field of 17.6 T to rule out any measurement artifacts and to confirm the estimated experimental uncertainty of the reported diffusion data. The observed agreement, within uncertainty, between the data at 17.6 T and 14 T in Figs. S5, S8, S9 that were measured under the same or similar experimental conditions using the same samples confirms the validity and reliability of the reported diffusion measurements.

It is seen in Figs. 1, 2, S5-S10 that the majority of the ^{13}C PFG NMR attenuation curves measured for methanol, ethanol, *p*-xylene and *o*-xylene diffusion in ZIF-71 crystal beds and ZIF-71/Torlon MMMs deviate from the monoexponential behavior corresponding to a single self-diffusivity for all sorbate molecules in a sample (Eq. (1)). The attenuation curves show a rapid decay at small q^2t values continued by a slower decay at larger q^2t values. This is a signature of the presence of at least two molecular ensembles of the same sorbate diffusing with different diffusivities in the studied samples. Indeed, it was observed that the measured non-monoexponential PFG NMR attenuation curves can be described by Eq. (3) assuming the existence of two molecular ensembles. The best fit curves using this equation are shown in the figures with the attenuation data, and the best fit parameters are presented in Tables S3–S6. The faster diffusing ensemble, i.e. ensemble 1, is attributed to the sorbate diffusion mostly outside of ZIF-71 crystals (for the crystals bed samples) or outside of the MMMs (for the MMM samples). The slower diffusing ensemble is assigned to the diffusion inside ZIF-71 crystals. This ensemble will be referred to as intra-ZIF ensemble or ensemble 2. It is important to note that no PFG NMR signal was observed from sorbate diffusion in the polymer phase of the MMMs. The lack of this signal is explained by small fractions of the intra-polymer ensemble of sorbate molecules in combination with the expectation of small ^{13}C T_2 NMR relaxation times of this ensemble. It was verified that no ^{13}C PFG NMR signal of the studied sorbate molecules can be observed for the intra-polymer phase in the samples prepared with pure Torlon films (no ZIF crystals added) under the identical or similar experimental conditions as those used for the MMM measurements. This result is fully expected in view of our previously reported data showing that no intra-polymer ^{13}C PFG NMR signal can be observed even for small gas molecules in the same polymer type [17,18,42].

In contrast to the samples with ZIF-71 beds and MMMs, ^{13}C PFG NMR attenuation curves measured at 14 T for reference samples of the bulk liquid sorbates (methanol, ethanol, *p*-xylene and *o*-xylene) without any porous material or polymer present show the monoexponential behavior (Eq. (1)) yielding a single, diffusion time independent diffusivity for each liquid (Fig. S11 and Table S7). These diffusivities are assigned to bulk liquid self-diffusivities.

3.2. Influence of ZIF crystal boundaries on the diffusion data

For ZIF-71 crystal beds it was observed that the fraction of intra-ZIF ensemble decreases as the diffusion time increases (Tables S3 and S4). Such fraction decrease can be explained by sorbate molecules leaving ZIF-71 crystals when these molecules reach the crystal boundaries, a behavior well-known from PFG NMR studies of zeolite beds [48,54] and more recent studies of ZIF and MOF beds [15,16,36,39]. Consequently, the fraction of ensemble 1 in the bed samples increases with diffusion time. This happens because with increasing time more and more sorbate molecules get a chance to escape ZIF-71 crystals and diffuse in the spaces between the crystals with a much higher diffusivity than that inside the crystals.

It was observed that the values of root MSDs calculated for intra-ZIF ensembles using Eq. (2) are similar to the average size of ZIF-71 crystals (Tables S3 and S4). This observation is consistent with the discussed above molecular exchange between the crystals and their surroundings in the bed samples under our experimental conditions. At sufficiently large diffusion times, when a significant fraction of molecules diffusing inside ZIF-71 crystals can reach the external crystal surface, the self-diffusivity of the intra-ZIF ensemble is expected to decrease with increasing root MSD and diffusion time [15–18,34,35,48]. This can happen due to reflections of diffusing molecules back into the crystals at the external crystal surface. It can also happen because "faster" molecules with larger displacements leave the crystals through the external crystal surface as they reach this surface. As a result, the remaining molecules would exhibit smaller diffusivity because the "faster" molecules that left the crystals could no longer contribute to the intra-ZIF ensemble. Such decrease in the self-diffusivity of the intra-ZIF ensemble with increasing root MSD and diffusion time was indeed observed for the bed samples (Figs. 3 and 4 and Tables S3 and S4) and it will be discussed in more detail later.

For ZIF-71/Torlon MMMs the observed change in the fractions of ensemble 1 with increasing diffusion time was much slower than that in the bed samples, or even non-existent, within uncertainty (Tables S5 and S6). This is attributed to the following two reasons. Firstly, at any particular time the fraction of sorbate molecules outside of MMMs in the MMM samples was significantly bigger than that outside of ZIF-71 crystals in the bed samples. Secondly, sorbate molecules that diffuse away from ZIF-71 crystals located in MMMs do not start contributing appreciably to ensemble 1 because they are expected to become "invisible" for PFG NMR as they cross over to the polymer phase. This is expected because of short ^{13}C T_2 NMR relaxation inside the polymer. For the same reasons as discussed above for ZIF-71 bed samples, the intra-ZIF self-diffusivity in the MMM samples is expected to decrease with increasing root MSD and diffusion time as more and more sorbate molecules reach the external crystal surface. Such decrease was indeed observed (Figs. 3 and 4 and Tables S5 and S6). It can be seen in Fig. 3 that the dependencies of the intra-ZIF self-diffusivity on root MSD for the MMMs with smaller batch B crystals is much stronger than those for the MMMs with large batch A crystals. Such difference is expected because for the same root MSD a larger fraction of sorbate molecules diffusing inside ZIF-71 crystals is expected to encounter the external crystal surface in the MMMs with smaller than with larger crystal sizes.

For ZIF-71/Torlon MMMs, a larger amount of liquid sorbate per unit mass of ZIF-71 crystals was added compared to ZIF-71 crystal beds to compensate for a possible long-time sorbate adsorption by Torlon. This resulted in larger fractions of ensemble 1 in ZIF-71/Torlon MMMs compared to ZIF-71 crystal beds (Figs. 1, 2, S7, S8, S9). Clearly, the condition of the sorption equilibration with a saturation vapor pressure of a sorbate is expected to be fulfilled for any non-zero amount of the sorbate in the liquid bulk phase of a sealed NMR sample. Nevertheless,

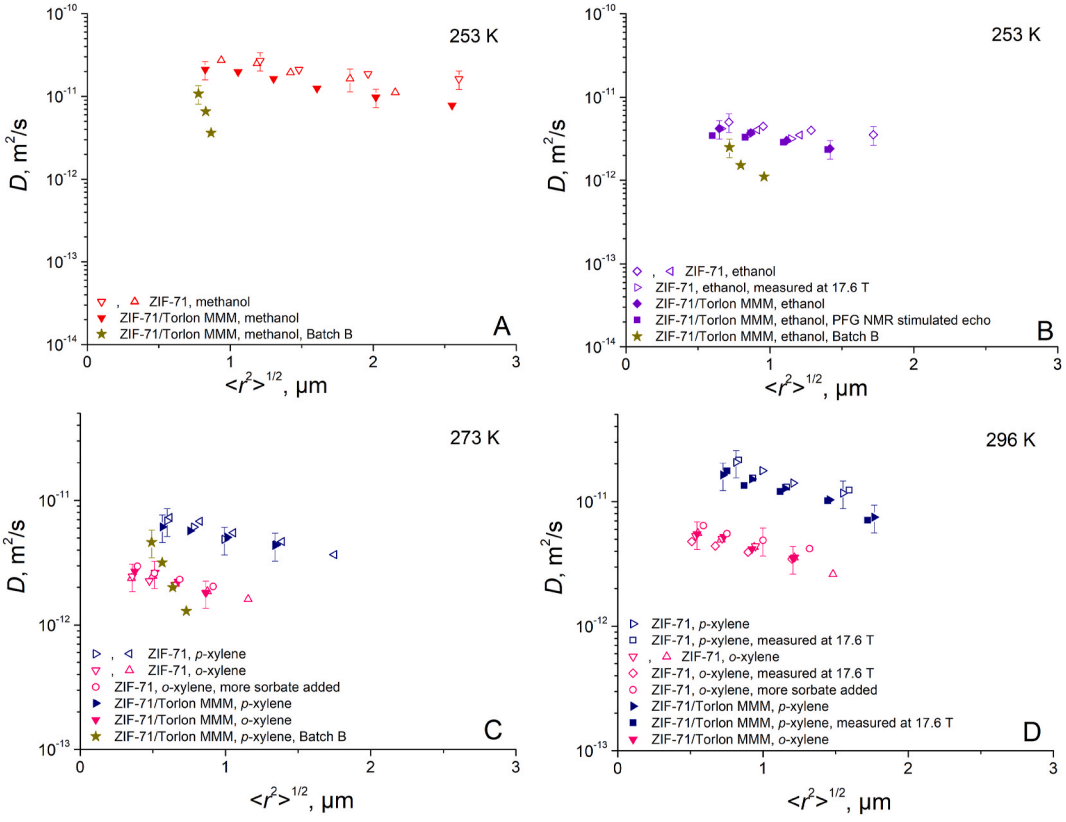

Fig. 3. Self-diffusivities of methanol (A), ethanol (B), *p*-xylene (C,D) and *o*-xylene (C,D) plotted as a function of root MSD for ZIF-71 crystal beds (hollow symbols) and ZIF-71/Torlon MMMs (filled symbols) at different temperatures shown in the figure. The data were measured for the samples containing ZIF-71 crystals with the average crystal size of 3 μm (batch A) by the 13-interval PFG NMR sequence at 14 T, unless indicated otherwise in the figure. In some cases, two identically prepared (but different) PFG NMR samples of ZIF-71 crystal beds were measured under the same experimental conditions.

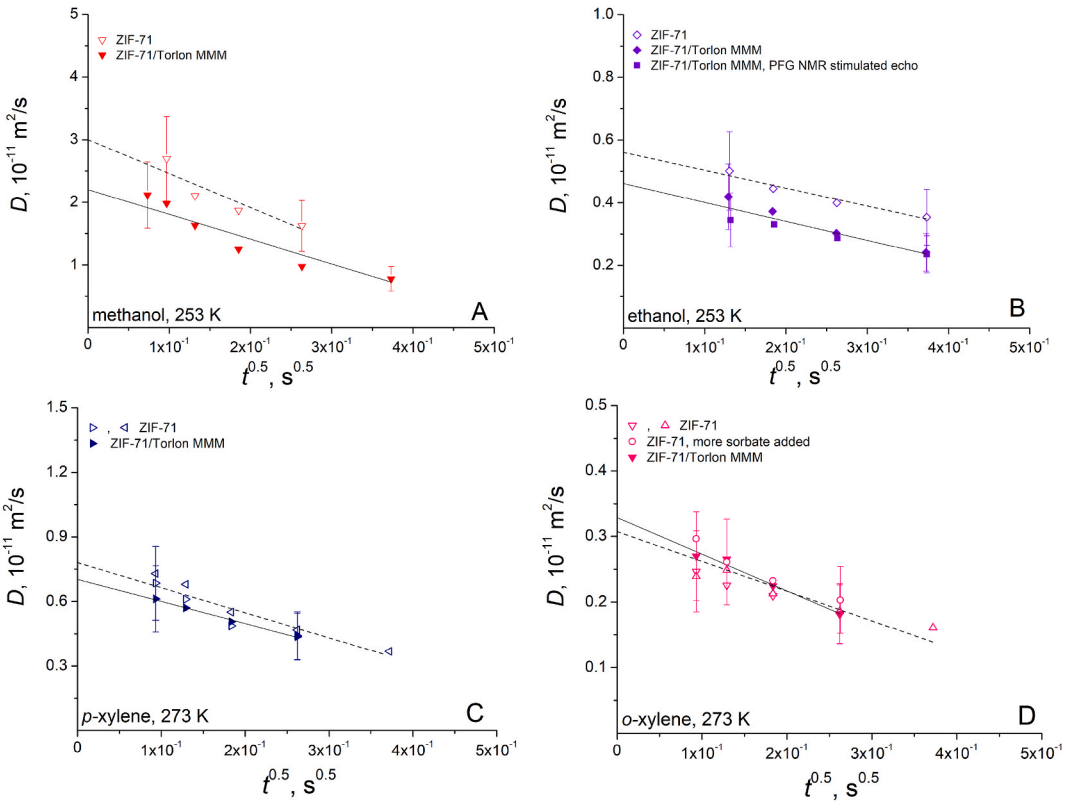

Fig. 4. Self-diffusivities of methanol (A), ethanol (B), *p*-xylene (C), and *o*-xylene (D) plotted as a function of $t^{0.5}$ for ZIF-71 crystal beds (empty symbols) and ZIF-71/Torlon MMM (filled symbols) samples for different temperatures of diffusion measurements shown in the figure. The dotted and solid lines show the results of least-square fitting using Eq. (4) for the bed and MMM data, respectively. The data were measured for the samples containing ZIF-71 crystals with the average crystal size of 3 μm (batch A) by the 13-interval PFG NMR sequence at 14 T, unless indicated otherwise. In some cases, two identically prepared (but different) PFG NMR samples of ZIF-71 crystal beds were measured under the same experimental conditions.

we verified that a significant increase in the fraction of ensemble 1 does not change the intra-ZIF diffusion data in the studied bed samples. In particular, an additional sample of ZIF-71 crystal bed was prepared with a significantly larger amount of *o*-xylene in a sealed NMR sample in comparison to the originally prepared sample. This additional sample was measured under the same experimental conditions as the ZIF-71 crystal bed prepared with the originally used lower total amount of *o*-xylene. As expected, within uncertainty, no difference was observed between the intra-ZIF self-diffusivities measured for any particular diffusion time in the two samples with different total amounts of *o*-xylene (Figs. 1D, 1E, S8B, S8C, and Table S4).

The measured dependencies of the intra-ZIF self-diffusion coefficients on diffusion time in the ZIF-71 bed and MMM samples can be used to obtain the intra-ZIF self-diffusivities (D_0), which are not perturbed by the discussed above effects at the external crystal surface. This can be done by using the equation proposed by Mitra et al. for self-diffusion inside porous spherical particles or crystals with radius (R) [55,56].

$$\frac{D(t)}{D_0} \approx 1 - \frac{f}{3R}\left(\frac{D_0 t}{\pi}\right)^{0.5}. \quad (4)$$

This equation is valid for both types of the influence of the external crystal surface discussed above, i.e. for the cases of (i) adsorbing boundaries when molecules leave the crystals upon encountering the external crystal surface ($f = 2$), and (ii) reflecting boundaries when molecules are reflected back into the crystals from the external crystal surface ($f = 4$). Eq. (4) was used to fit the measured dependencies of the intra-ZIF self-diffusivities on diffusion time ($D(t)$) to obtain the values of D_0 for each studied sample, as discussed below. However, owing to the broad distributions over crystal sizes in both studied batches of ZIF-71 crystals (Fig. S1), and the related uncertainty in the values of f, it was not possible to analyze the type of influence of the external surface on the intra-ZIF self-diffusion using Eq. (4).

Figs. 4–5 and S12 present the intra-ZIF self-diffusivities plotted as a function of square root of the diffusion time for the samples of ZIF-71 crystal beds and ZIF-71/Torlon MMMs. The straight and dotted lines in the figures show the least square fits using Eq. (4) for the MMM and bed samples, respectively. The intercepts of the lines with the vertical axes yield the values of D_0, viz. intra-ZIF self-diffusivities not influenced by any effects at the crystal boundaries. Table 2 summarizes the values of D_0, while Table 3 shows the ratios of these values obtained for each sorbate pair (methanol/ethanol or *p*-xylene/*o*-xylene) under the same conditions in the ZIF-71 crystal beds and in the corresponding ZIF-71/Torlon MMMs.

3.3. Comparison of intra- ZIF self-diffusivities in MMMs and crystal beds

It can be seen in Table 2 and Figs. 4 and S12 that for the same sorbate and under the same measurement conditions there is an agreement, within uncertainty, between the values of D_0 for the bed and MMM samples prepared with large (batch A) ZIF-71 crystals. The data in Table 2 and Fig. 5 indicate that although the D_0 values in the MMMs with large (batch A) ZIF-71 crystals show a tendency to be slightly larger than the corresponding diffusivities in the MMMs with small (batch B) ZIF-71 crystals, the observed difference is within the experimental uncertainty in all cases. Hence, we can conclude that the confinement of ZIF-71 crystals in Torlon to form ZIF-71/Torlon MMMs did not lead to any appreciable differences in the values of D_0. It is important to note that the confinement of ZIF-11 crystals in the same polymer type was shown to lead to a reduction in the intra-ZIF self-diffusivity of gas molecules,

Table 2
Intra-ZIF self-diffusivities in the limit of small diffusion times (D_0) at 253 K, 273 K and 296 K obtained by fitting the PFG NMR data with Eq. (4) for ZIF-71 crystal beds and ZIF-71/Torlon MMMs.

Sample	T (K)	Average crystal size of ZIF-71 (μm)	D_0 (10^{-10} m^2/s)
ZIF-71 loaded with methanol	253	3	0.30 ± 0.08
ZIF-71 loaded with ethanol	253	3	0.056 ± 0.014
ZIF-71 loaded with *p*-xylene	273	3	0.079 ± 0.020
ZIF-71 loaded with *o*-xylene	273	3	0.031 ± 0.007
ZIF-71 loaded with *p*-xylene	296	3	0.25 ± 0.06
ZIF-71 loaded with *o*-xylene	296	3	0.064 ± 0.016
ZIF-71/Torlon MMM loaded with methanol	253	3	0.22 ± 0.06
ZIF-71/Torlon MMM loaded with methanol	253	1	0.18 ± 0.05
ZIF-71/Torlon MMM loaded with ethanol	253	3	0.046 ± 0.013
ZIF-71/Torlon MMM loaded with ethanol	253	1	0.035 ± 0.009
ZIF-71/Torlon MMM loaded with *p*-xylene	273	3	0.070 ± 0.018
ZIF-71/Torlon MMM loaded with *p*-xylene	273	1	0.055 ± 0.014
ZIF-71/Torlon MMM loaded with *o*-xylene	273	3	0.033 ± 0.008
ZIF-71/Torlon MMM loaded with *p*-xylene	296	3	0.19 ± 0.05
ZIF-71/Torlon MMM loaded with *o*-xylene	296	3	0.067 ± 0.018

Table 3
Diffusion selectivities, i.e. the ratios of the intra-ZIF self-diffusivities in the limit of small diffusion times (D_0) for ZIF-71 crystal beds and ZIF-71/Torlon MMMs. The data correspond to ZIF-71 crystals with average crystal size of 3 μm (batch A), unless indicated otherwise.

sorbate 1/ sorbate 2	T (K)	Ratios of D_0 values for ZIF-71 beds[b] ($D_{0,\ sorbate\ 1}/D_{0,\ sorbate\ 2}$)	Ratios of D_0 values for ZIF-71/Torlon MMMs[b] ($D_{0,\ sorbate\ 1}/D_{0,\ sorbate\ 2}$)
Methanol/ ethanol	253	5.4	4.8
Methanol/ ethanol	253	–	4.3[a]
p-xylene/*o*-xylene	273	2.6	2.1
p-xylene/*o*-xylene	296	3.9	2.8

[a] ZIF-71/Torlon MMM containing ZIF-71 crystals with the average crystal size of 1 μm (batch B).
[b] 35% experimental uncertainty.

but only at the gas loadings inside ZIF-11 crystals significantly lower than the maximum loadings [17,18]. In the limit of large gas loadings there was no such self-diffusivity reduction. The diffusivity decrease observed at the low gas loadings was attributed to a reduction in the framework flexibility of ZIF-11 crystals due to the crystal confinement in Torlon. It is important to note that there is a significant evidence in the literature on the possibility of ZIF and MOF framework flexibility reduction caused by polymer confinement [7,15–18,42,43,57]. The previously reported absence of the influence of the confinement in Torlon on intra-ZIF gas self-diffusivity at large gas loadings was explained by possible polymer plasticization and/or crowding of sorbate molecules in ZIF crystals that reduces the ZIF framework flexibility even without any confinement in the polymer [17,18,42]. Owing to the fact that the current study was performed in the limit of large sorbate loadings corresponding to the sorption equilibrium with the sorbates at the saturation vapor pressure, it is not surprising that no noticeable difference between the rates of intra-ZIF self-diffusion in unconfined and polymer-confined ZIF crystals was observed. To explore the confinement effect further, our future studies with liquid sorbates will focus on MMMs with crosslinked polymers, which are less likely to exhibit plasticization effects, and/or with sorbates at lower loadings.

It is important to note that the reported intra-ZIF diffusion data show diffusion selectivity for the studied methanol/ethanol and *p*-xylene/*o*-xylene sorbate pairs. It can be seen in Tables 2 and 3 that for both the ZIF bed and MMM samples the D_0 values for methanol (~ 3.6 Å [58]) are larger by a factor of about 4–5 than those for ethanol (~ 4.5 Å [58]) under the same or similar experimental conditions. Similarly, these Tables show that the D_0 values for *p*-xylene (5.8 Å [58]) are larger than those for *o*-xylene (6.8 Å [58]) by a factor of about 2–4, depending on the temperature and measurement conditions. The diffusion selectivity (viz. ratio of the intra-ZIF self-diffusivities for different sorbates) is mostly based on molecular sieving due to passages through ZIF-71 apertures with a nominal size of 4.2 Å [19]. This size is smaller than that of some of the sorbate molecules used in this study. Clearly, framework flexibility of ZIF-71 leads to larger effective aperture sizes that play a significant role in the molecular sieving process. We expect the diffusion selectivities to become larger if ZIF-71 framework flexibility is reduced by the polymer confinement, as discussed above.

4. Conclusion

^{13}C PFG NMR at 14 T was utilized to measure self-diffusivities of methanol, ethanol, *p*-xylene and *o*-xylene inside ZIF-71 crystals that were either confined in Torlon polymer and served as a filler in ZIF-71/Torlon MMMs or were loosely packed to form crystal beds without any confinement. Selected ^{13}C PFG NMR measurements were also performed at a larger field of 17.6 T. The observed coincidence of the data measured with the same samples at different magnetic field strengths and otherwise the same conditions was used to rule out any possible measurement artifacts. The intra-ZIF self-diffusivities in ZIF-71/Torlon MMMs and in the corresponding ZIF-71 beds were found to decrease with increasing diffusion time and the corresponding root MSD. The observed diffusivity dependencies were attributed to an influence of the external crystal surface on trajectories of the diffusing molecules, which reach this surface. The quantitative analysis of the diffusion time dependent self-diffusivities resulted in the intra-ZIF self-diffusivities (D_0) that were not perturbed by the influence of the external crystal surface. For each studied sorbate, no difference, within the experimental error, was observed between the values of D_0 measured under the same or similar conditions in ZIF-71/Torlon MMMs and in the corresponding ZIF-71 beds. This result shows that there is no influence of confinement of ZIF-71 crystals in Torlon polymer on the intra-ZIF self-diffusion for the studied liquids. The absence of such influence was discussed in the context of the previously published data showing the effect of the ZIF confinement in Torlon on intra-ZIF self-diffusivities of gas molecules at gas loadings well below the saturation loadings in ZIF crystals. For the studied liquids, the lack of an effect of confinement of ZIF-71 crystals in Torlon polymer on D_0 was attributed to molecular crowding and/or Torlon plasticization, which are possible at high loadings of liquid sorbates.

To our knowledge, this work represents the first study demonstrating direct measurement of self-diffusion and self-diffusion selectivity of liquid sorbates inside MOF crystals located in polymer-based MMMs. Direct access to diffusion data for liquids inside MOF crystals in MMMs is required for knowledge-based design of such MMMs for liquid separations, which can be influenced by diffusion changes due to crystal boundary effects and/or reduction in the framework flexibility of MOF crystals.

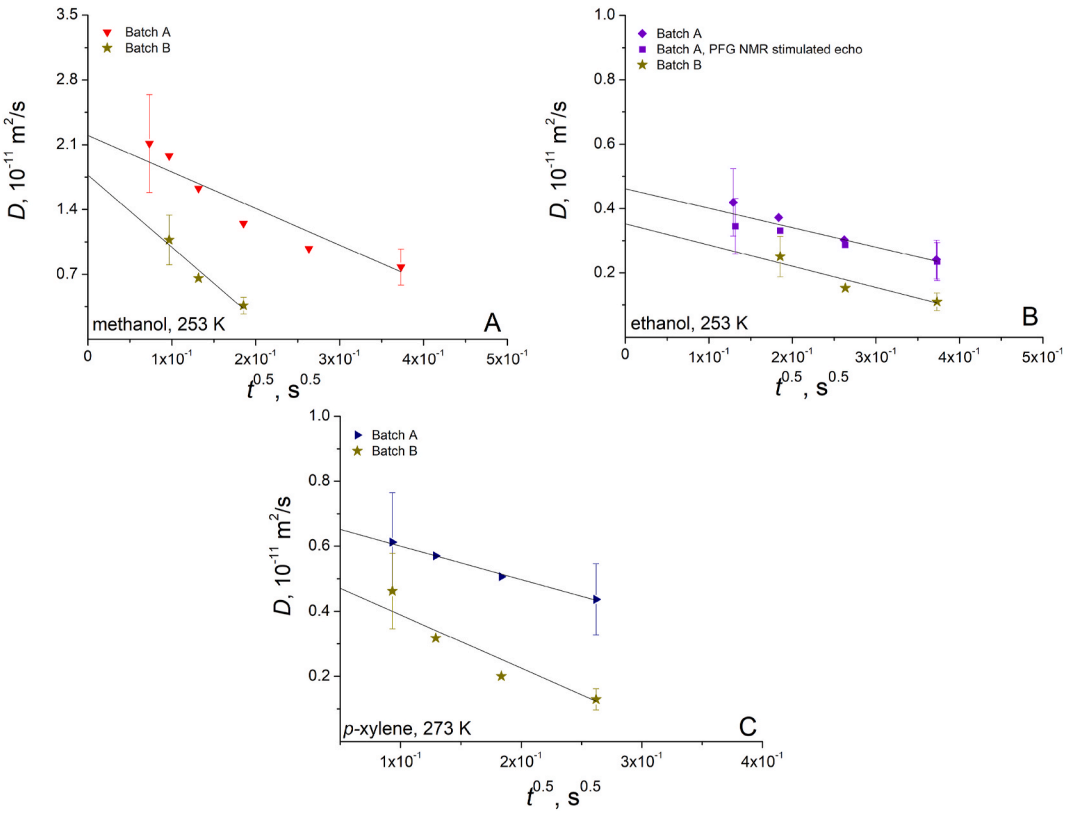

Fig. 5. Self-diffusivities of methanol (A), ethanol (B) and *p*-xylene (C) plotted as a function of $t^{0.5}$ for ZIF-71/Torlon MMM samples prepared with ZIF-71 crystals with average crystal sizes of 3 μm (Batch A) and 1 μm (Batch B). The solid lines show the results of least-square fitting using Eq. (4). The data were measured by ^{13}C PFG NMR at 14 T and different temperatures indicated in the figure.

Author statement

All authors of this manuscript declare that this manuscript is original, has not been published before and is not currently being considered for publication elsewhere. The manuscript has been read and approved by all named authors and that there are no other persons who satisfied the criteria for authorship but are not listed. The order of authors listed in the manuscript has been approved by all authors. The Corresponding Author is the sole contact for the Editorial process. He is responsible for communicating with the other authors about progress, submissions of revisions and final approval of proofs.

Amineh Baniani – Data curation, Formal analysis, Investigation, Validation, Writing - original draft
Matthew P. Rivera – Data curation, Formal analysis, Investigation, Writing - review and editing
Ryan P. Lively – Funding acquisition, Methodology, Project administration, Supervision, Resources, Writing - review and editing
Sergey Vasenkov - Funding acquisition, Methodology, Project administration, Resources, Supervision, Validation, Writing - original draft

Declaration of competing interest

The authors declare that they have no known competing financial interests or personal relationships that could have appeared to influence the work reported in this paper.

Acknowledgments

The present work was financially supported by NSF (CBET awards No. 1836735 and No. 1836738). A portion of this work was performed in the McKnight Brain Institute at the National High Magnetic Field Laboratory's AMRIS Facility, which is supported by National Science Foundation Cooperative Agreement No. DMR-1157490 and the State of Florida. This work was supported in part by an NIH award, S10RR031637, for magnetic resonance instrumentation.

Appendix A. Supplementary data

Supplementary data to this article can be found online at https://doi.org/10.1016/j.memsci.2021.119786.

References

[1] N. Habib, Z. Shamair, N. Tara, A.-S. Nizami, F.H. Akhtar, N.M. Ahmad, M.A. Gilani, M.R. Bilad, A.L. Khan, Development of highly permeable and selective mixed matrix membranes based on Pebax®1657 and NOTT-300 for CO_2 capture, Separ. Purif. Technol. (2020) 234.
[2] S. Quan, S.W. Li, Y.C. Xiao, L. Shao, CO_2-Selective mixed matrix membranes (MMMs) containing graphene oxide (GO) for enhancing sustainable CO_2 capture, Int. J. Greenh. Gas Con. 56 (2017) 22–29.
[3] C.I. Chaidou, G. Pantoleontos, D.E. Koutsonikolas, S.P. Kaldis, G. P. Sakellaropoulos, Gas separation properties of polyimide-zeolite mixed matrix membranes, Separ. Sci. Technol. 47 (2012) 950–962.
[4] M. Maghami, A. Abdelrasoul, Zeolite mixed matrix membranes (Zeolite-MMMs) for sustainable engineering, in: Zeolites and Their Applications, 2018.
[5] R.T. Adams, J.S. Lee, T.-H. Bae, J.K. Ward, J.R. Johnson, C.W. Jones, S. Nair, W. J. Koros, CO_2–CH_4 permeation in high zeolite 4A loading mixed matrix membranes, J. Membr. Sci. 367 (2011) 197–203.
[6] A.F. Ismail, W.R. Rahman, F. Aziz, Development of polysulfone (PSF)-Carbon molecular sieve (CMS) mixed matrix membrane (MMM) for O_2/N_2 gas separation, AIP Conf. Proc. 1136 (2009) 201–206.
[7] L. Diestel, N. Wang, B. Schwiedland, F. Steinbach, U. Giese, J. Caro, MOF based MMMs with enhanced selectivity due to hindered linker distortion, J. Membr. Sci. 492 (2015) 181–186.
[8] M.S. Boroglu, A.B. Yumru, Gas separation performance of 6FDA-DAM-ZIF-11 mixed-matrix membranes for H_2/CH_4 and CO_2/CH_4 separation, Separ. Purif. Technol. 173 (2017) 269–279.

[9] R.C. Dutta, S.K. Bhatia, Interfacial engineering of MOF-based mixed matrix membrane through atomistic simulations, J. Phys. Chem. C 124 (2020) 594–604.
[10] T. Li, Y. Pan, K.-V. Peinemann, Z. Lai, Carbon dioxide selective mixed matrix composite membrane containing ZIF-7 nano-fillers, J. Membr. Sci. 425–426 (2013) 235–242.
[11] G. Yilmaz, S. Keskin, Predicting the performance of zeolite imidazolate framework/polymer mixed matrix membranes for CO_2, CH_4, and H_2 separations using molecular simulations, Ind. Eng. Chem. Res. 51 (2012) 14218–14228.
[12] S. Saqib, S. Rafiq, N. Muhammad, A.L. Khan, A. Mukhtar, S. Ullah, M.H. Nawaz, F. Jamil, C. Zhang, V. Ashokkumar, Sustainable mixed matrix membranes containing porphyrin and polysulfone polymer for acid gas separations, J. Hazard Mater. 411 (2021).
[13] A.S. Wiryoatmojo, H.A. Mannan, R. Nasir, H. Mukhtar, D.F. Mohshim, A. Abdulrahman, Z. Man, Surface modification effect of carbon molecular sieve (CMS) on the morphology and separation performance of mixed matrix membranes, Polym. Test. 80 (2019), 106152.
[14] D. Qadir, H. Mukhtar, L.K. Keong, Synthesis and characterization of polyethersulfone/carbon molecular sieve based mixed matrix membranes for water treatment application, Procedia Eng. 148 (2016) 588–593.
[15] R. Mueller, S. Zhang, C. Zhang, R.P. Lively, S. Vasenkov, Relationship between long-range diffusion and diffusion in the ZIF-8 and polymer phases of mixed-matrix membrane by high field NMR diffusometry, J. Membr. Sci. 477 (2015) 123–130.
[16] R. Mueller, V. Hariharan, C. Zhang, R. Lively, S. Vasenkov, Relationship between mixed and pure gas self-diffusion for ethane and ethene in ZIF-8/6FDA-DAM mixed-matrix membrane by pulsed field gradient NMR, J. Membr. Sci. 499 (2016) 12–19.
[17] E.M. Forman, A. Baniani, L. Fan, K.J. Ziegler, E. Zhou, F. Zhang, R.P. Lively, S. Vasenkov, Ethylene diffusion in crystals of zeolitic imidazole Framework-11 embedded in polymers to form mixed-matrix membranes, Microporous Mesoporous Mater. 274 (2019) 163–170.
[18] E.M. Forman, A. Baniani, L. Fan, K.J. Ziegler, E. Zhou, F. Zhang, R.P. Lively, S. Vasenkov, Relationship between ethane and ethylene diffusion inside ZIF-11 crystals confined in polymers to form mixed-matrix membranes, J. Membr. Sci. 593 (2020).
[19] B.R. Pimentel, A. Parulkar, E.-k. Zhou, N.A. Brunelli, R.P. Lively, Zeolitic imidazolate frameworks: next-generation materials for energy-efficient gas separations, Chem. Sustain. Energy Mater. 7 (2014) 3202–3240.
[20] P.A. Banerjee R, B. Wang, C. Knobler, H. Furukawa, M. O'Keeffe, O.M. Yaghi, High-throughput synthesis of zeolitic imidazolate frameworks and application to CO2 capture, Science 319 (2008) 939–943.
[21] K.S. Park, Z. Ni, A.P. Côté, J.Y. Choi, R. Huang, F.J. Uribe-Romo, H.K. Chae, M. O'Keeffe, O.M. Yaghi, Exceptional chemical and thermal stability of zeolitic imidazolate frameworks, Proc. Natl. Acad. Sci. Unit. States Am. 103 (2006) 10186–10191.
[22] S. Sorribas, P. Gorgojo, C. Téllez, J. Coronas, A.G. Livingston, High flux thin film nanocomposite membranes based on metal–organic frameworks for organic solvent nanofiltration, J. Am. Chem. Soc. 135 (2013) 15201–15208.
[23] G.M. Shi, T. Yang, T.S. Chung, Polybenzimidazole (PBI)/Zeolitic imidazolate frameworks (ZIF-8) mixed matrix membranes for pervaporation dehydration of alcohols, J. Membr. Sci. 415–416 (2012) 577–586.
[24] S. Basu, M. Maes, A. Cano-Odena, L. Alaerts, D.E.D. Vos, I.F.J. Vankelecom, Solvent resistant nanofiltration (SRNF) membranes based on metal-organic frameworks, J. Membr. Sci. 344 (2009) 190–198.
[25] C. Zhang, Y. Dai, J.R. Johnson, O. Karvan, W.J. Koros, High performance ZIF-8/6FDA-DAM mixed matrix membrane for propylene/propane separations, J. Membr. Sci. 389 (2012) 34–42.
[26] H. An, K.Y. Cho, S. Back, X.H. Do, J.-D. Jeon, H.K. Lee, K.-Y. Baek, J.S. Lee, The significance of the interfacial interaction in mixed matrix membranes for enhanced propylene/propane separation performance and plasticization resistance, Separ. Purif. Technol. (2021) 261.
[27] T.-H. Bae, J.S. Lee, W. Qiu, W.J. Koros, C.W. Jones, S. Nair, A high-performance gas-separation membrane containing submicrometer-sized metal-organic framwork crystals, Angew. Chem. Int. Ed. 49 (2010) 9863–9866.
[28] J. Sánchez-Laínez, B. Zornoza, Á. Mayoral, Á. Berenguer-Murcia, Diego Cazorla-Amorós, C. Téllez, J. Coronas, Beyond the H_2/CO_2 upper bound: one-step crystallization and separation of nano-sized ZIF-11 by centrifugation and its application in mixed matrix membranes, J. Mater. Chem. 3 (2015) 6549–6556.
[29] S. Japip, Y. Xiao, T.-S. Chung, Particle-size effects on gas transport properties of 6FDA-durene/ZIF-71 mixed matrix membranes, Ind. Eng. Chem. Res. 55 (2016) 9507–9517.
[30] Y. Li, L.H. Wee, J.A. Martens, I.F.J. Vankelecom, ZIF-71 as a potential filler to prepare pervaporation membranes for bio-alcohol recovery, J. Mater. Chem. 2 (2014) 10034–10040.
[31] S. Liu, G. Liu, X. Zhao, W. Jin, Hydrophobic-ZIF-71 filled PEBA mixed matrix membranes for recovery of biobutanol via pervaporation, J. Membr. Sci. 446 (2013) 181–188.
[32] H. Yin, C.Y. Lau, M. Rozowski, C. Howard, Y. Xu, T. Lai, M.E. Dose, R.P. Lively, M. L. Lind, Free-standing ZIF-71/PDMS nanocomposite membranes for the recovery of ethanol and 1-butanol from water through pervaporation, J. Membr. Sci. 529 (2017) 286–292.
[33] W. Morris, B. Leung, H. Furukawa, O.K. Yaghi, N. He, H. Hayashi, Y. Houndonougbo, M. Asta, B.B. Laird, O.M. Yaghi, A combined Experimental−Computational investigation of carbon dioxide capture in a series of isoreticular zeolitic imidazolate frameworks, J. Am. Chem. Soc. 132 (2010) 11006–11008.
[34] A. Baniani, C. Chmelik, E.M. Forman, L. Fan, K.J. Ziegler, E. Zhou, F. Zhang, R. Lyndon, R.P. Lively, S. Vasenkov, Anomalous relationship between molecular size and diffusivity of ethane and ethylene inside crystals of zeolitic imidazolate framework-11, J. Phys. Chem. C 123 (2019) 16813–16822.
[35] E.M. Forman, B.R. Pimentel, K.J. Ziegler, R.P. Lively, S. Vasenkov, Microscopic diffusion of pure and mixed methane and carbon dioxide in ZIF-11 by high field diffusion NMR, Microporous Mesoporous Mater. 248 (2017) 158–163.
[36] A.-K. Pusch, T. Splith, L. Moschkowitz, S. Karmakar, R. Biniwale, M. Sant, G. B. Suffritti, P. Demontis, J. Cravillon, E. Pantatosaki, F. Stallmach, NMR studies of carbon dioxide and methane self-diffusion in ZIF-8 at elevated gas pressures, Adsorption 18 (2012) 359–366.
[37] S. Berens, F. Hillman, H.-K. Jeong, S. Vasenkov, Self-diffusion of pure and mixed gases in mixed-linker zeolitic imidazolate framework-7-8 by high field diffusion NMR, Microporous Mesoporous Mater. 288 (2019), 109603.
[38] C. Zhang, R.P. Lively, K. Zhang, J.R. Johnson, O. Karvan, W.J. Koros, Unexpected molecular sieving properties of zeolitic imidazolate framework-8, J. Phys. Chem. Lett. 3 (2012) 2130–2134.
[39] S. Berens, F. Hillman, M.R.A. Hamid, H.-K. Jeong, SergeyVasenkov, influence of 2-ethylimidazole linker-doping in ZIF-8 crystals on intracrystalline self-diffusion of gas molecules by high field diffusion NMR, Microporous Mesoporous Mater. 315 (2021), 110897.
[40] M.V. Parkes, H. Demir, S.L. Teich-McGoldrick, D.S. Sholl, J.A. Greathousea, M. D. Allendorfc, Molecular dynamics simulation of framework flexibility effects on noble gas diffusion in HKUST-1 and ZIF-8, Microporous Mesoporous Mater. 194 (2014) 190–199.
[41] J. Park, M. Agrawal, D.F.S. Gallis, J.A. Harvey, J.A. Greathouse, D.S. Sholl, Impact of intrinsic framework flexibility for selective adsorption of sarin in non-aqueous solvents using metal–organic frameworks, Phys. Chem. Chem. Phys. 22 (2020) 6441–6448.
[42] A. Baniani, S.J. Berens, M.P. Rivera, R.P. Lively, S. Vasenkov, Potentials and Challenges of High-Field PFG NMR Diffusion Studies with Sorbates in Nanoporous Media, Adsorption (2020).
[43] S. Friebe, A. Mundstock, K. Volgmann, J. Caro, On the better understanding of the surprisingly high performance of Metal−Organic framework-based mixed-matrix membranes using the example of UiO-66 and matrimid, ACS Appl. Mater. Interfaces 9 (2017) 41553–41558.
[44] R.P. Lively, M.E. Dose, J.A. Thompson, B.A. McCool, R.R. Chance, W.J. Koros, Ethanol and water adsorption in methanol-derived ZIF-71, Chem. Commun. 47 (2011) 8667–8669.
[45] M. Dvoyashkin, J. Zang, G.I. Yucelen, A. Katihar, S. Nair, D.S. Sholl, C.R. Bowers, S. Vasenkov, Diffusion of tetrafluoromethane in single-walled aluminosilicate nanotubes: pulsed field gradient NMR and molecular dynamics simulations, J. Phys. Chem. C 116 (2012) 21350–21355.
[46] R.M. Cotts, M.J.R. Hoch, T. Sun, J.T. Markert, Pulsed field gradient stimulated echo methods for improved NMR diffusion measurements in heterogeneous systems, J. Magn. Reson. 83 (1989) 252–266.
[47] S.J. Gibbs, C.S. Johnson, A PFG NMR experiment for accurate diffusion and flow studies in the presence of eddy currents, J. Magn. Reson. 93 (1991) 395–402.
[48] J. Kärger, D.M. Ruthven, D.N. Theodorou, Diffusion in Nanoporous Materials, Wiley-VCH Verlag GmbH & Co. KGaA, Weinheim, Germany, 2012.
[49] J. Kärger, H. Pfeifer, W. Heink, Principles and application of self-diffusion measurements by NMR, Adv. Magn. Reson. 12 (1988) 1–89.
[50] J. Kärger, M. Avramovska, D. Freude, J. Haase, S. Hwang, R. Valiullin, Pulsed Field Gradient NMR Diffusion Measurement in Nanoporous Materials, Adsorption, 2020.
[51] P.T. Callaghan, D. MacGowan, K.J. Packer, F.O. Zelaya, Influence of field gradient strength in NMR studies of diffusion in porous media, Magn. Reson. Imaging 9 (1991) 663–671.
[52] E.O. Stejskal, J.E. Tanner, Spin diffusion measurements: spin echoes in the presence of a time-dependent field gradient, J. Chem. Phys. 42 (1965) 288–292.
[53] P. Galvosas, F. Stallmach, G. Seiffert, J. Kärger, U. Kaess, G. Majer, Generation and application of ultra-high-intensity magnetic field gradient pulses for NMR spectroscopy, J. Magn. Reson. 151 (2001) 260–268.
[54] O. Geier, R.Q. Snurr, F. Stallmach, J. Kärger, Boundary effects of molecular diffusion in nanoporous materials: a pulsed field gradient nuclear magnetic resonance study, J. Chem. Phys. 120 (2004) 367.
[55] P.P. Mitra, P.N. Sen, Effects of microgeometry and surface relaxation on NMR pulsed-field-gradient experiments: simple pore geometries, Phys. Rev. B 45 (1992) 143–156.
[56] P.P. Mitra, P.N. Sen, L.M. Schwartz, Short-time behavior of the diffusion coefficient as a geometrical probe of porous media, Phys. Rev. B 47 (1993) 8565–8574.
[57] L. Sheng, C. Wang, F. Yang, L. Xiang, X. Huang, J. Yu, L. Zhang, Y. Pan, Y. Li, Enhanced C_3H_6/C_3H_8 separation performance on MOF membranes through blocking defects and hindering framework flexibility by silicone rubber coating, Chem. Commun. 53 (2017) 7760–7763.
[58] J.-R. Li, R.J. Kuppler, H.-C. Zhou, Selective gas adsorption and separation in metal–organic frameworks, Chem. Soc. Rev. 38 (2009) 1477–1504.